Check for updates

Special Issue Article

Advances in Mechanical Engineering

Advances in Mechanical Engineering
2015, Vol. 7(6) 1–7
© The Author(s) 2015
DOI: 10.1177/1687814015589721
aime.sagepub.com
SAGE

Microstructure, phase transformation and hardness of nanometric Cr-Al multilayer coatings

Yean-Liang Su[1], Kai-Wen Cheng[1], Joachim Mayer[2], Thomas E Weirich[2], Alexander Schwedt[2] and Yue-Feng Lin[1]

Abstract

Nanometric Cr-Al multilayer films are deposited by magnetron sputtering to investigate the influences of composition and annealing on the microstructure, phase transformation, and hardness. The enhancement of hardness of as-deposited coatings is attributed to solid solution strengthening and grain size strengthening. For the $Cr_{100-x}Al_x$ coatings with $x = 30$ at.% and $x = 62$ at.%, respectively, the annealing process prompts the formation of Cr_2Al and Cr_5Al_8 intermetallic compounds. The enhancement of hardness of annealed coatings is primarily caused by the intermetallic formation and secondarily by oxide layer formation.

Keywords

Alloys, materials mechanical properties, material behavior, structures, nanostructures

Date received: 26 January 2015; accepted: 20 April 2015

Academic Editor: Xiaotun Qiu

Introduction

Cr-Al alloys find application in various fields including the aerospace industry and other high-temperature environments due to their low specific weight and high thermal stability.[1] In addition, Cr-Al films have high electrical resistivity and excellent heat resistance and are therefore ideally suited to the fabrication of highly integrated electronic components.[2] Moreover, Al alloys and Al-based intermetallic coatings have high hardness and good corrosion resistance and are thus widely used for corrosion protection in aggressive environments. Previous studies have shown that the microhardness of Al coatings can be increased to 10 GPa through the addition of transition metals in suitable quantities, for example, 20 at.% Cr.[3] Furthermore, salt bath results have shown that Cr-Al coatings with 18 at.% Cr have excellent corrosion resistance (i.e. more than 800 h without corrosion)[4] In addition, Cr-Al intermetallic compounds (IMCs) such as Cr_2Al and Cr_5Al_8 act as reservoir phases of Cr and Al, and hence contribute toward protective scale formation.[5] Various methods have been proposed for preparing Cr-Al IMCs, including levitation induction melting,[6] mechanical alloying,[7] mechanically activated annealing,[8] laser surface alloying,[9] and vacuum fusing.[10]

Nanoscale multilayer films have attracted significant interest due to their many favorable mechanical, structural, optical and electronic properties. Many intermetallics of Al/TM have been prepared via the heat

[1]Department of Mechanical Engineering, National Cheng-Kung University, 701 Tainan, Taiwan
[2]Central Facility for Electron Microscopy GFE, RWTH Aachen University, 52074 Aachen, Germany

Corresponding author:
Yue-Feng Lin, Department of Mechanical Engineering, National Cheng Kung University, 701 Tainan, Taiwan.
Email: n18981408@mail.ncku.edu.tw

Creative Commons CC-BY: This article is distributed under the terms of the Creative Commons Attribution 3.0 License (http://www.creativecommons.org/licenses/by/3.0/) which permits any use, reproduction and distribution of the work without further permission provided the original work is attributed as specified on the SAGE and Open Access pages (http://www.uk.sagepub.com/aboutus/openaccess.htm).

treatment of nanoscale multilayer films, including Al/Pd,[11] Al/Ti,[12] Al/Ni,[13] Al/Mg,[14] Al/Cu,[15] and Al/Ru.[16] However, the literature lacks a detailed investigation into the microstructure and phase transformation of nanometric Cr-Al multilayers before and after heat treatment. Accordingly, this study investigates the effects of Al addition and annealing on the microstructure, phase transformation, and hardness of nanometric Cr-Al multilayer films.

Experiment

Nanometric Cr-Al multilayer films were deposited on AISI M2 steel substrates by magnetron sputtering at room temperature. Four rectangular targets were installed around the cylindrical deposition chamber. To obtain the desired overall chemical composition ($Cr_{100-x}Al_x$, $x = 14$ to 62 at.%), the Cr targets were operated at a constant $1.2 \times 10^{-2}\,W\,mm^{-2}$, while the power of the Al target was adjusted as required. The targets were powered by a constant direct current (DC) supply, whereas the substrate was biased with a pulsed DC supply. A Cr interlayer with a thickness of approximately 80 nm was deposited prior to the sputtering of the Cr-Al films. Multilayer Cr-Al films with a bilayer period of approximately 12 nm were produced by varying the rotation speed of the substrate turntable. The total thickness of the bilayer films was around 2.5–3.0 μm. To form Cr-Al alloy coatings, the as-deposited multilayer films were heated from room temperature to 600 °C over a period of 1 h under ambient conditions. The phase constitutions, crystal structures, chemical compositions, and microstructures of the as-deposited and annealed films were characterized by means of X-ray diffraction (XRD), field emission scanning electron microscopy (FESEM), energy-dispersive spectroscopy (EDS), scanning transmission electron microscopy (STEM), and glow discharge optical emission spectroscopy (GDOS). In addition, the nanoindentation hardness of the films was measured using a Micro Materials NanoTest System equipped with a Berkovich diamond indenter. In performing the nanoindentation tests, the initial load was set as 0.01 mN, the maximum load as 5 mN, the loading and unloading rate as 0.05 mN s^{-1}, and the dwell time under maximum load as 10 s.

Figure 1(a) shows a typical cross-sectional STEM micrograph and EDS line-scan profile of the as-deposited $Cr_{70}Al_{30}$ multilayer film. Note that the darker layers are Al, whereas the lighter layers are Cr. The micrograph confirms the presence of an alternating multilayer structure with a bilayer period of approximately 12 nm. The multilayer structure has offsets of Cr and Al concentrations in the Cr-rich and Al-rich layers, respectively, and the Al and Cr concentrations are not zero. These findings suggest the occurrence of co-deposition during the sputtering process. Figure 1(b) shows a bright-field cross-sectional transmission electron microscopy (TEM) image of the as-deposited $Cr_{70}Al_{30}$ sample. The selected area diffraction (SAD) pattern presented in the inset shows the presence of only body-centered cubic (bcc) Cr rings. However, strong concentration fluctuations and the individual layers of the bilayer structure are still visible, indicating the dissolution of the Al into the bcc Cr matrix with non-uniform solubility. Figure 1(c) and (d) shows the STEM micrograph, EDS line-scan profile, bright-field cross-sectional TEM image, and SAD pattern of the $Cr_{70}Al_{30}$ multilayer film annealed at 600 °C. Under elevated temperature conditions, the Cr and Al elements diffuse into one another more readily, and hence the multilayered structure is less distinct. Moreover, the SAD pattern shows only Cr_2Al rings, and hence it is inferred that the Cr and Al react completely to form Cr_2Al IMC under high-temperature conditions.

Figure 2(a) shows the XRD patterns of the as-deposited Cr-Al multilayer films with various Al contents. The Cr films deposited without Al content are highly crystalline with larger crystallites, indicating a Cr phase with strong (110) and (200) orientations. For the films with an Al content of less than 30 at.%, the spectra contain only Cr peaks. In other words, the Al dissolves fully into the bcc Cr matrix. This observation is consistent with the findings of Chakrabarti and Beck[17] that the maximum solubility of Al and Cr in bulk alloy is 30.7 at.%. Al phases are also detected when the overall Al content increases to 52 or 62 at.% because the solubility is more than 30.7 at.%. The position of Cr(110) peaks gradually shifts toward the lower diffraction angle as the Al content increases (inset of Figure 2(a)). This result can be attributed to the increase in the interplanar spacing (d-spacing) of the Cr(110) crystal planes. The increase in d-spacing is caused by the formation of solid solution in the Cr/Al multilayer films whereby Cr atoms are substituted by Al atoms. This is because the radius of Al (0.1431 nm) is larger than that of Cr (0.1249 nm). Figure 2(b) shows a linear relationship between Al content and peak position, lattice constant, and d-spacing as the overall Al content increases from 0 to 30 at.%. These results are in agreement with Vegard's[18] law for solid solutions. The Cr(110) peak profiles in the inset of Figure 2(a) also show an increase in the peak width and a decrease in the peak intensity as the Al content increases. This result could be attributed to two factors. The first factor is the non-uniform lattice distortion of the Cr lattice, which is due to the dissolution of Al in Cr with a non-uniform and non-stoichiometry solubility (Figure 1(a)). The second factor is the reduction of crystallite size (Figure 2(c)). The crystallite size was determined using the Williamson–Hall method[19] and the Lorentzian peak profiles. The crystallite sizes of Cr were calculated from Cr(110) and (200) peaks in all samples, and those of Al were

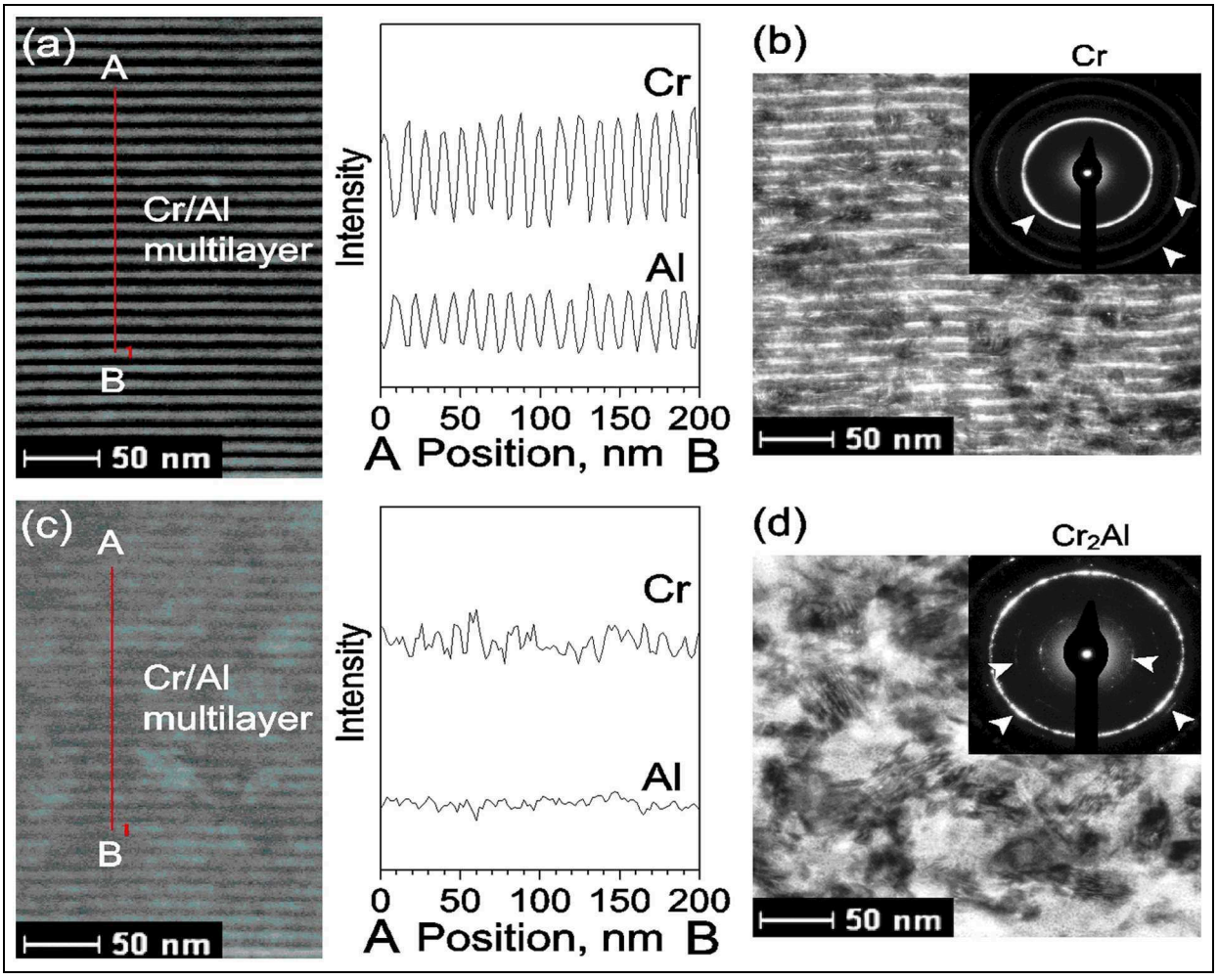

Figure 1. STEM cross-sectional images and EDS line scans from A to B of (a) as-deposited and (c) annealed (600 °C, 1 h) $Cr_{70}Al_{30}$ multilayer films. Bright-field cross-sectional TEM images of (b) as-deposited and (d) annealed (600 °C, 1 h) $Cr_{70}Al_{30}$ multilayer films. Note that the insets in (b) and (d) show the corresponding selected area diffraction patterns.

calculated from all Al peaks in $Cr_{48}Al_{52}$ and $Cr_{38}Al_{62}$ samples. The crystallite size of Cr decreased significantly from 347 to 60 nm as the overall Al content increased from 0 to 30 at.%. Further increasing Al content from 30 to 62 at.% left the crystallite size of Cr almost unchanged. However, the crystallite size of Cr remained almost unchanged when the overall Al content exceeded 62 at.%. The crystallite sizes of Al in $Cr_{48}Al_{52}$ and $Cr_{38}Al_{62}$ are 126 and 141 nm, respectively.

Figure 2(d) shows the XRD patterns of the Cr-Al multilayer thin films annealed at 600 °C with different overall Al content. After annealing, Cr and Cr_2O_3 phases appeared in the pure Cr films. The appearance of the Cr_2O_3 phase indicates the formation of an oxide layer. The thickness of this oxide (i.e. the depth of oxygen diffusion from the surface) is approximately 600 nm (according to GDOS). The intensity of Cr_2O_3 peaks decreases as the Al content increases. The Cr_2Al, Cr, and Cr_2O_3 phases appear in $Cr_{76}Al_{24}$ films. The formation of this new phase is caused by the reaction of Cr and Al. When the overall Al content reaches 30 at.%, Cr and Al react completely, and only diffraction peaks from Cr_2Al are detected. These results are in agreement with the SAD results shown in Figure 1(d). The disappearance of the Cr_2O_3 phase and the depth of oxygen diffusion of only 50 nm (using the energy-filtered transmission electron microscopy (EFTEM) elemental mapping for oxygen) suggest that $Cr_{70}Al_{30}$ films have an excellent oxidation resistance. In $Cr_{48}Al_{52}$ films, the Cr_5Al_8 phase appears in addition to Cr_2Al. When the overall Al content reaches 62 at.%, only the Cr_5Al_8 phase is apparent. Before and after annealing at 600 °C in atmosphere for 1 h, the reactions on $Cr_{100-x}Al_x$ multilayer films with a bilayer period of 12 nm and various overall Al contents ($x = 0$ to 62) can be summarized as follows

$$x = 0 \text{ and } 14 : Cr + Al \rightarrow Cr(Al)_{ss} \rightarrow Cr(Al)_{ss} + Cr_2O_3$$

$$x = 24 : Cr + Al \rightarrow Cr(Al)_{ss} \rightarrow Cr(Al)_{ss} + Cr_2O_3 + Cr_2Al$$

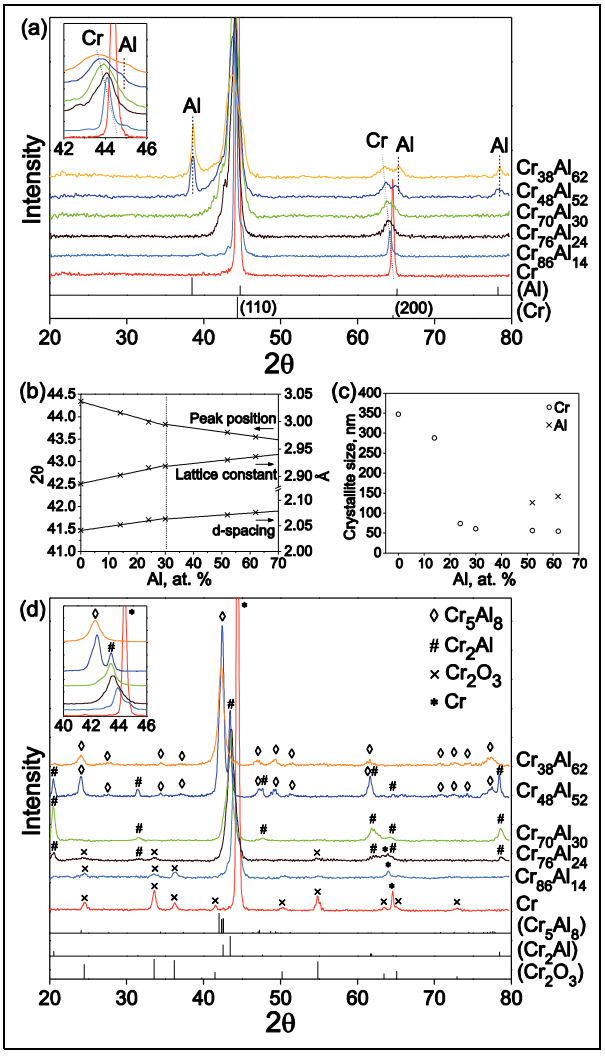

Figure 2. (a) Standard XRD spectra of Cr and Al and measured XRD patterns of as-deposited $Cr_{100-x}Al_x$ multilayer films. Note that the inset shows an enlarged view of the spectra in the vicinity of Cr(110). (b) Plots of peak position, lattice constant, and d-spacing of Cr(110) as function of Al content. (c) Effect of Al content on crystallite size. (d) Standard XRD spectra for Cr_2O_3, Cr_2Al, and Cr_5Al_8 and measured XRD patterns of annealed $Cr_{100-x}Al_x$ multilayer films. Note that the inset shows an enlarged view of the spectra in the vicinity of Cr(110).

$$x = 30 : \mathrm{Cr} + \mathrm{Al} \rightarrow \mathrm{Cr(Al)_{ss}} \rightarrow \mathrm{Cr_2Al}$$

$$x = 52 : \mathrm{Cr} + \mathrm{Al} \rightarrow \mathrm{Cr(Al)_{ss}} + \mathrm{Al} \rightarrow \mathrm{Cr_2Al} + \mathrm{Cr_5Al_8}$$

$$x = 62 : \mathrm{Cr} + \mathrm{Al} \rightarrow \mathrm{Cr(Al)_{ss}} + \mathrm{Al} \rightarrow \mathrm{Cr_5Al_8}$$

where $Cr(Al)_{ss}$ represents a solid solution of Al dissolved in Cr. These results are consistent with the phase diagram.[20]

Figure 3 shows the cross-sectional structure of the Cr-Al multilayer films using FESEM. The fracture cross-section of the pure Cr coating has obvious and undamaged columnar grains that grow larger as they approach the surface. The average width of the columnar grains close to the surface is approximately 400 nm. After annealing at 600 °C, compared to the as-deposited films, the fracture mode changes from an intergranular fracture to an intragranular fracture during the preparation of cross-sectional samples. As the Al content increases, the columnar structure becomes slender and less obvious. This means that the addition of a small amount of Al hinders the growth of chrome columnar grains, making the grains more compact and refined. When the overall Al content reaches 30 at.%, the columnar grains disappear and evolve into small and closely packed equiaxed grains, and the surface becomes smoother. The average diameters of the grains of as-deposited and annealed $Cr_{70}Al_{30}$ films are approximately 50 and 70 nm, respectively. However, further increasing the concentration of Al reduces the coating compactness and increases the grain size. When the overall Al content reaches 62 at.%, the grain sizes of the as-deposited and annealed films increase to 80 and 110 nm, respectively. The tendencies of the grain size measurements obtained from the scanning electron microscopy (SEM) images are in good general agreement with the values calculated from the XRD patterns. However, it is noted that the measured grain sizes are larger than (or equal to) the calculated values since one grain may actually contain several crystals.

Figure 4(a) presents EFTEM elemental mappings of the as-deposited and annealed $Cr_{70}Al_{30}$ multilayer films. The images indicate a uniform distribution of the Cr elements throughout both the coatings, and the annealed $Cr_{70}Al_{30}$ multilayer film has an oxygen diffusion depth of approximately 60 nm. Figure 4(b) shows the hardness values of the as-deposited and annealed films and the oxygen diffusion depth (as measured again by EFTEM elemental mapping) as a function of the Al content. It is seen that the oxygen diffusion depth has a maximum value of approximately 600 nm in the annealed samples. However, the diffusion depth reduces notably as the Al content increases. The hardness of the as-deposited pure Cr coating is around 2.0 GPa. As the Al content is increased to 30 at.%, the hardness increases significantly to around 26.8 GPa. However, as the Al content is further increased, the hardness reduces. As discussed earlier, Al phases are present in the multilayer films with Al contents of 52 or 62 at.% since full solubility of the Al into the Cr matrix is impossible for additions greater than 30.7 at.%. For the maximum Al content of 62.4 at.%, the hardness decreases notably to 6.4 GPa. Comparing these results to the previous results presented for the solid solution and crystallite size suggests that two factors are responsible for the variation in the hardness of the as-deposited coatings. The first factor is that of solid solution strengthening, in which the maximum hardness is achieved when the overall concentration of Al reaches

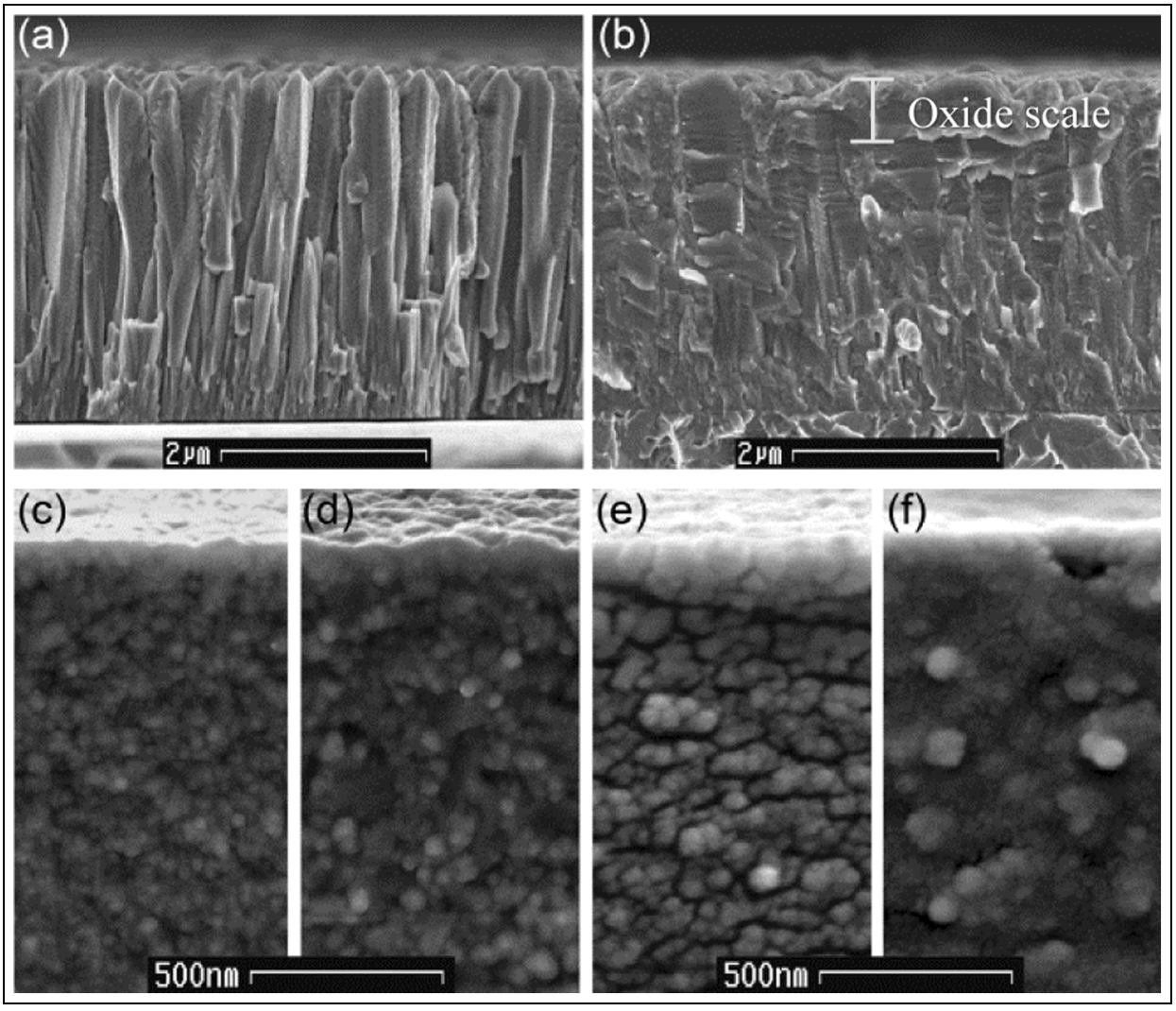

Figure 3. Cross-sectional SEM images of as-deposited $Cr_{100-x}Al_x$ multilayer films with (a) $x = 0$ at.%, (c) $x = 30$ at.%, and (e) $x = 62$ at.% and annealed $Cr_{100-x}Al_x$ multilayer films with (b) $x = 0$ at.%, (d) $x = 30$ at.%, and (f) $x = 62$ at.%.

the maximum solid solubility (i.e. 30.7 at.%). The second factor is that of grain size strengthening, in which the hardness decreases as the Al content increases beyond 30.7 at.% due to the precipitation of large Al crystallites. The results in Figure 4(b) show that annealing increases the hardness of all the samples. For the pure Cr film, the hardness increases only slightly from 2.0 to 3.6 GPa despite the presence of a thick oxide layer (i.e. 600 nm). However, a more substantial enhancement of the hardness occurs in the films containing Cr_2Al and/or Cr_5Al_8 IMCs despite the relatively lower thickness of the oxide layer (i.e. 50–70 nm). In general, the results suggest that the improved hardness of the coatings following annealing is the result primarily of the formation of Cr_2Al and Cr_5Al_8 IMCs and, to a lesser extent, oxide layer formation. However, further research is required to determine the exact nature of the oxide formed on the surface (i.e. Cr_2O_3, Al_2O_3, or mixed oxide) and to explore further possible mechanisms for the enhanced hardness, such as dislocation movement.

Summary

Nanometric Cr-Al multilayer films with a bilayer period of approximately 12 nm have been deposited on AISI M2 steel substrates. The effects of the Cr-Al composition and elevated temperature annealing on the microstructure, phase transformation, and hardness of the films have been examined by means of XRD, FESEM, EDS, STEM, GDOS, and nanoindentation testing. For an Al content of less than 30 at.%, the XRD spectra show the presence of only Cr peaks (i.e. no Al peaks are observed). However, as the Al content increases to 52 or 62 at.%, Al phases are detected since the Al content is greater than the maximum solubility limit for Al in

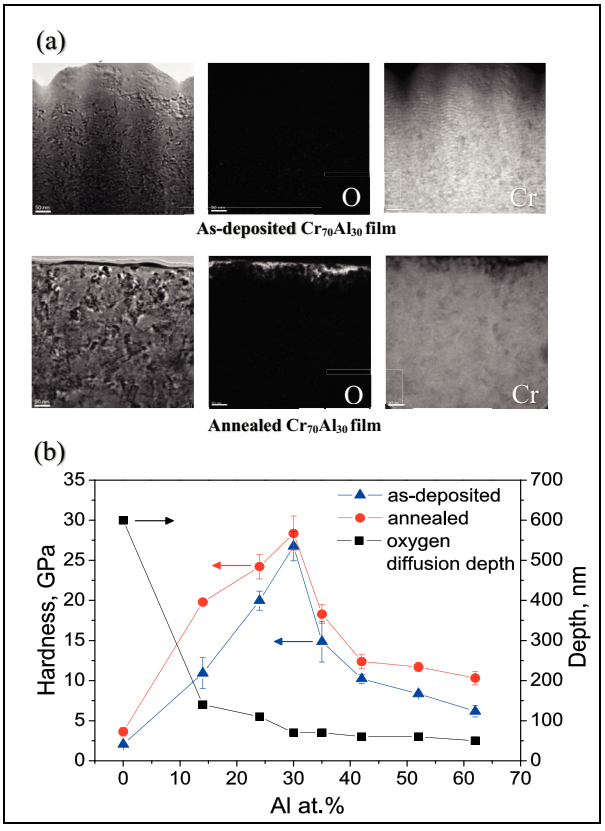

Figure 4. (a) EFTEM elemental mappings of as-deposited $Cr_{70}Al_{30}$ film (upper) and annealed $Cr_{70}Al_{30}$ multilayer film (lower). (b) Effect of Al content on hardness and oxygen diffusion depth in $Cr_{100-x}Al_x$ multilayer films.

Cr (i.e. 30.7 at.%). For the annealed $Cr_{100-x}Al_x$ coatings with $x = 30$ at.% and $x = 62$ at.%, a reaction of the Cr and Al occurs, resulting in the formation of Cr_2Al and Cr_5Al_8 IMCs in the multilayer film. The hardness of the as-deposited pure Cr coating is equal to just 2.0 GPa. However, for an Al content of 30 at.%, the hardness increases to 26.8 GPa. The enhancement in the hardness of the as-deposited coatings is attributed to solid solution strengthening and grain size strengthening. Irrespective of the Al content, the annealed coatings exhibit a greater hardness than the as-deposited samples. The improved hardness is the result primarily of Cr-Al intermetallic formation and, to a lesser extent, the presence of an oxide layer.

Declaration of conflicting interests

The authors declare that there is no conflict of interest.

Funding

The authors would like to express their gratitude to the Ministry of Science and Technology, Taiwan, for the financial support of this study under Contract No. NSC 101-2221-E-006-021-MY3.

References

1. Vojtěch D, Verner J, Šerák J, et al. Properties of thermally stable PM Al-Cr based alloy. *Mater Sci Eng A Struct* 2007; 458: 371–380.
2. Ozawa PJ, Yoshizaki S, Takeyama S, et al. Electrical properties of Cr-Al alloy thin films. *IEEE Trans Compon Hybr* 1986; 9: 391–395.
3. Sanchette F and Billard A. Main features of magnetron sputtered aluminum-transition metal alloy coatings. *Surf Coat Technol* 2001; 142–144: 218–224.
4. Creus J, Billard A and Sanchette F. Corrosion behaviour of amorphous Al-Cr and Al-Cr-(N) coatings deposited by dc magnetron sputtering on mild steel substrate. *Thin Solid Films* 2004; 466: 1–9.
5. Guo MH, Wang QM, Ke PL, et al. The preparation and hot corrosion resistance of gradient NiCoCrAlYSiB coatings. *Surf Coat Technol* 2006; 200: 3942–3949.
6. Grushko B, Przepiórzyński B and Pavlyuchkov D. On the constitution of the high-Al region of the Al-Cr alloy system. *J Alloy Compd* 2008; 454: 214–220.
7. Shamah AM, Ibrahim S and Hanna FF. Formation of nano quasicrystalline and crystalline phases by mechanical alloying. *J Alloy Compd* 2011; 509: 2198–2202.
8. Archana MS, Hebalkar N, Radha K, et al. Phase formation during mechanically activated annealing of nanocrystalline Cr-60 at.% Al. *J Alloy Compd* 2010; 501: 18–24.
9. Almeida A and Vilar R. Al-Al7Cr eutectic in Al-Cr alloys synthesized by laser alloying. *Scripta Mater* 2010; 63: 811–814.
10. Zhou W, Zhao YG, Qin QD, et al. A new way to produce Al + Cr coating on Ti alloy by vacuum fusing method and its oxidation resistance. *Mater Sci Eng A Struct* 2006; 430: 254–259.
11. Ramos AS and Vieira MT. Intermetallic compound formation in Pd/Al multilayer thin films. *Intermetallics* 2012; 25: 70–74.
12. Ramos AS, Vieira MT, Morgiel J, et al. Production of intermetallic compounds from Ti/Al and Ni/Al multilayer thin films-a comparative study. *J Alloy Compd* 2009; 484: 335–340.
13. Gachon J-C, Rogachev AS, Grigoryan HE, et al. On the mechanism of heterogeneous reaction and phase formation in Ti/Al multilayer nanofilms. *Acta Mater* 2005; 53: 1225–1231.
14. Kim JS, LaGrange T, Reed BW, et al. Direct characterization of phase transformations and morphologies in moving reaction zones in Al/Ni nanolaminates using dynamic transmission electron microscopy. *Acta Mater* 2011; 59: 3571–3580.
15. Oliva AI, Corona JE and Sosa V. AlCu alloy films prepared by the thermal diffusion technique. *Mater Charact* 2010; 61: 696–702.
16. Zotov N, Woll K and Mücklich F. Phase formation of B2-RuAl during annealing of Ru/Al multilayers. *Intermetallics* 2010; 18: 1507–1516.
17. Chakrabarti DJ and Beck PA. Transport properties of Cr-A1 solid solutions. *J Phys Chem Solid* 1971; 32: 1609–1615.
18. Vegard L. Die Konstitution der Mischkristalle und die Raumffillung der Atome. *Z Phys* 1921; 5: 17–26.

19. Williamson GK and Hall WH. X-ray line broadening from filed aluminium and wolfram. *Acta Metall* 1953; 1: 22–31.
20. Mahdouk K and Gachon J-C. Thermodynamic investigation of the aluminum-chromium system. *J Phase Equilib* 2000; 21: 157–166.